Positive and negative signal and line shape in stimulated Raman spectroscopy: Resonance femtosecond Raman spectra of diphenylbutadiene

A. L. Dobryakov,[1] O. A. Krohn,[2] M. Quick,[1,a)] I. N. Ioffe,[3,a)] and S. A. Kovalenko[1,a)]

AFFILIATIONS

[1] Department of Chemistry, Humboldt-Universität zu Berlin, Brook-Taylor-Str. 2, D-12489 Berlin, Germany
[2] Department of Physics and of Chemistry, University of Colorado, Boulder, Colorado 80309-0215, USA
[3] Department of Chemistry, Lomonosov Moscow State University, Moscow, Russia

[a)]**Authors to whom correspondence should be addressed:** martinquick@hotmail.de; ioffe@phys.chem.msu.ru; and skovale@chemie.hu-berlin.de

ABSTRACT

Resonance stimulated Raman signal and line shape are evaluated analytically under common electronic/vibrational dephasing and exponential Raman/probe pulse, $\exp(-|t|/\tau)$. Generally, the signal from a particular state includes contributions from higher and lower electronic states. Thus, with $S_0 \rightarrow S_1$ actinic excitation, the Raman signal consists of 15 Feynman diagrams entering with different signs. The negative sign indicates vibrational coherences in S_1 or higher S_n, whereas the positive sign reveals coherences in S_0 or S_n via $S_1 \rightarrow S_n \rightarrow S_m$ ($n < m$) coupling. The signal complexity is in contrast to spontaneous Raman with its single diagram only. The results are applied to femtosecond stimulated Raman spectra of trans–trans, cis–trans (ct), and cis–cis (cc) 1,4-diphenyl-1,3-butadiene, the ct and cc being reported for the first time. Upon actinic excitation, the Stokes spectra show negative bands from S_1 or S_n. When approaching higher resonances $S_n \rightarrow S_m$, some Raman bands switch their sign from negative to positive, thus, indicating new coherences in S_n. The results are discussed, and the measured Raman spectra are compared to the computed quantum-chemical spectra.

I. INTRODUCTION

Femtosecond stimulated Raman (FSR) spectroscopy is a powerful tool for probing photoinduced molecular rearrangements. Proposed by Yoshizawa in 1994,[1] the technique has been largely developed by the group of Mathies[2–9] and his collaborators[10–21] as well as by other researchers.[22–36] The technique is unique, as it combines high temporal (femtosecond) and high spectral (several cm^{-1}) resolutions. This is in contrast to conventional spontaneous Raman[37] where the temporal resolution is limited by the picosecond Raman pulse. The trade-off is the complexity of the FSR signal that generally contains both positive and negative contributions,[30] a result not recognized in previous theoretical reports.[4,7,10–13,23,34]

In early FSR experiments,[6,7,16,22] researchers noticed a variety of Raman line shapes that may change in the vicinity of electronic resonances from symmetric to dispersive shape or even switch the sign of the signal. The features were explained by inverse Raman and hot luminescence contributions,[7,10,11,17] by resonance-dependent Franck–Condon activity,[22] or by the interplay between pulse parameters and intramolecular dynamics.[23,24] The theoretical analysis assumed vibrational coherences in actinically excited state S_1 and in lower S_0 or higher state S_n.[10–13,16,17] However, it was not considered that these coherences may contribute to different signs. In particular, without actinic excitation, resonance stimulated Raman spectra contain negative contributions from S_0 and positive and negative contributions from S_1.[30,31]

In this paper, we focus on the above issues. We provide a detailed procedure for calculating the excited-state FSR signal in the resonance case. For simplicity, we consider here only the Stokes spectra, as the generalization to the anti-Stokes case is straightforward and detailed in the supplementary material. We also pay attention to the similarity between transient absorption (TA) and stimulated Raman in connection with their spontaneous counterparts, fluorescence, and spontaneous Raman.

The theoretical analysis is illustrated by experimental FSR spectra of trans–trans (tt), cis–trans (ct), and cis–cis (cc) 1,4-diphenyl-1,3-butadiene (DPB). The first Raman spectra of this compound were calculated[38] and measured[39–46] in 1980–1990, but the excited-state spectra were recorded only in a high frequency range >600 cm^{-1} and only for the tt-isomer.

II. TRANSIENT ABSORPTION VS STIMULATED RAMAN

It is necessary to stress a deep similarity between TA and FSR spectroscopy.[28–31] They both deliver a stimulated signal of differential absorption ΔA, which is usually measured in mOD units, with 1 mOD = 0.001 ln 10. The difference between the techniques is only that the TA results from the pump and probe, while the FSR comes from an actinic pump and simultaneously acting Raman and probe. It is, therefore, advantageous to measure the FSR signal in the mOD units as well.[28–31] This is different from a common approach for measuring the Raman signal, the conversion to conventional Raman gain/loss units being given by

$$1\ \text{mOD} = 0.0023(\text{gain/loss}). \tag{1}$$

Importantly, the sign of ΔA may be positive or negative. We follow the convention from TA spectroscopy, where ΔA is positive for absorption and negative for emission and bleach. Since the non-resonant Stokes FSR signal appears in emission, it should be considered negative, while the corresponding anti-Stokes absorptive signal is positive. Recall that this definitio is opposite to that of common Raman literature, where the Raman gain is taken to be positive.

It is also instructive to compare TA and FSR with regard to their spontaneous counterparts. For TA, this is time-resolved flu orescence. The latter appears in TA as stimulated emission (SE), but there are also two other contributions, bleach and excited-state absorption (ESA). Similarly, for FSR, there is a term corresponding to spontaneous Raman from S_1, but there are many others in the resonance case. These additional contributions result from lower S_0 and higher S_n electronic states since the Raman and probe field are capable of creating vibrational coherences there.

III. CALCULATING THE FSR SIGNAL

Nonlinear spectroscopic signals can be calculated with the response function formalism developed by Mukamel and coworkers.[47–50] The basic concepts and key definitions from Refs. 47–54 are adapted here.

The femtosecond stimulated Raman signal is treated within the fifth-order perturbation formalism. A useful approximation assumes well separated in time pump and probe pulses with delay t between them. The actinic pump prepares the system with population p in S_1. Delayed Raman E_R and probe E fields induce the optical changes in the third-order approximation. The sequential contribution (E_R, E_R, E) generates a Raman background that should be subtracted. We focus on the coherent contribution $A^{(3)}$ arising from Raman and probe fields and resulting in a background-free Raman signal. The quantity of interest is the transient signal $\Delta A^{(5)}(\omega, t)$ induced by the actinic pulse and probed upon delay t by the Raman and probe pulses as functions of probe frequency ω.

The FSR signal in the probe direction $\mathbf{k} + \mathbf{k_R} - \mathbf{k_R}$ is then given by[47,48,50,52]

$$\Delta A^{(5)}(\omega, t) = p(t)\Delta A^{(3)}(\omega) = p(t)\mathrm{Im}\left(P^{(3)}(\omega)/E\right), \tag{2}$$

where population $p(t)$, created by the actinic pump, evolves in time, while Raman polarization $P^{(3)}$ is given by triple integration and summation over all possible paths,

$$P^{(3)}(\omega) = \sum_{[s]} \int_0^\infty dt_3 \int_0^\infty dt_2 \int_0^\infty dt_1 R^{(3)}_{[s]}(t_3, t_2, t_1) \times FT\left(E^{(3)}_{[s]}(t, t_3, t_2, t_1)\right), \tag{3}$$

where $R^{(3)}_{[s]}(t_3, t_2, t_1)$ is the nonlinear response, FT is the Fourier transform, and the nonlinear fiel $E^{(3)}_{[s]}$ depends on the ordering of Raman E_R and probe E,

$$E^{(3)}_{\alpha}(t, t_3, t_2, t_1) = E_R(t - t_3)E(t - t_3 - t_2){E_R}^*(t - t_3 - t_2 - t_1), \tag{4a}$$

$$E^{(3)}_{\beta}(t, t_3, t_2, t_1) = E_R(t - t_3){E_R}^*(t - t_3 - t_2)E(t - t_3 - t_2 - t_1), \tag{4b}$$

with [s] = α or β. Assuming a common electronic/vibrational dephasing rate Γ, the response function is given by

$$R^{(3)}_{[s]}(t_3, t_2, t_1) = -iM_{[s]} \exp(-i\tilde{\omega}_{mn}t_3 - i\tilde{\omega}_{kl}t_2 - i\tilde{\omega}_{pq}t_1), \tag{5}$$

where $\tilde{\omega}_{ab} = (\omega_{ab} - i\Gamma_{ab})$, $\omega_{ab} = (\varepsilon_a - \varepsilon_b)$, and Γ_{ab} is the dephasing rate between states $|a\rangle$ and $|b\rangle$. The path $[s]$ is specifie by subscripts (mn, kl, pq), and $M_{[s]}$ is the product of the transition dipole moments along the path. The Fourier transform gives

$$FT\left(E^{(3)}_{\alpha}\right) = \exp(i\omega t_3 + i(\omega - \Omega_R + i/\tau_R)t_2 - i(\Omega_R - i/\tau_R)t_1), \tag{6a}$$

$$FT\left(E^{(3)}_{\beta}\right) = \exp(i\omega t_3 + i(\omega - \Omega_R + i/\tau_R)t_2 - i(\omega + 2i/\tau_R)t_1). \tag{6b}$$

The triple integration in (3) can be done analytically with exponential pulses $E_R(t) \sim \exp\left(-\frac{|t|}{\tau_R} - i\Omega_R t\right)$ and $E(t) \sim \exp\left(-\frac{|t|}{\tau} - i\omega t\right)$. Upon integration with $\tau \ll \tau_R$ and omitting $p(t)$ and the nonlinearity index, the FSR signal is given by

$$\Delta A(\omega) = -\sum_{[s]} M_{[s]}\sigma^{(s)} \cdot \mathrm{Im}\left\{f_{mn} \cdot g_{kl} \cdot h^s_{pq}\right\}, \tag{7a}$$

$$f_{mn} = 1/(\omega - \tilde{\omega}_{mn}), \quad g_{kl} = i/(\omega - \Omega_R - \tilde{\omega}_{kl} + i/\tau_R), \tag{7b}$$

$$h^{\alpha}_{pq} = -i/(\Omega_R + \tilde{\omega}_{pq}), \quad h^{\beta}_{pq} = i/(\omega - \tilde{\omega}_{pq}). \tag{7c}$$

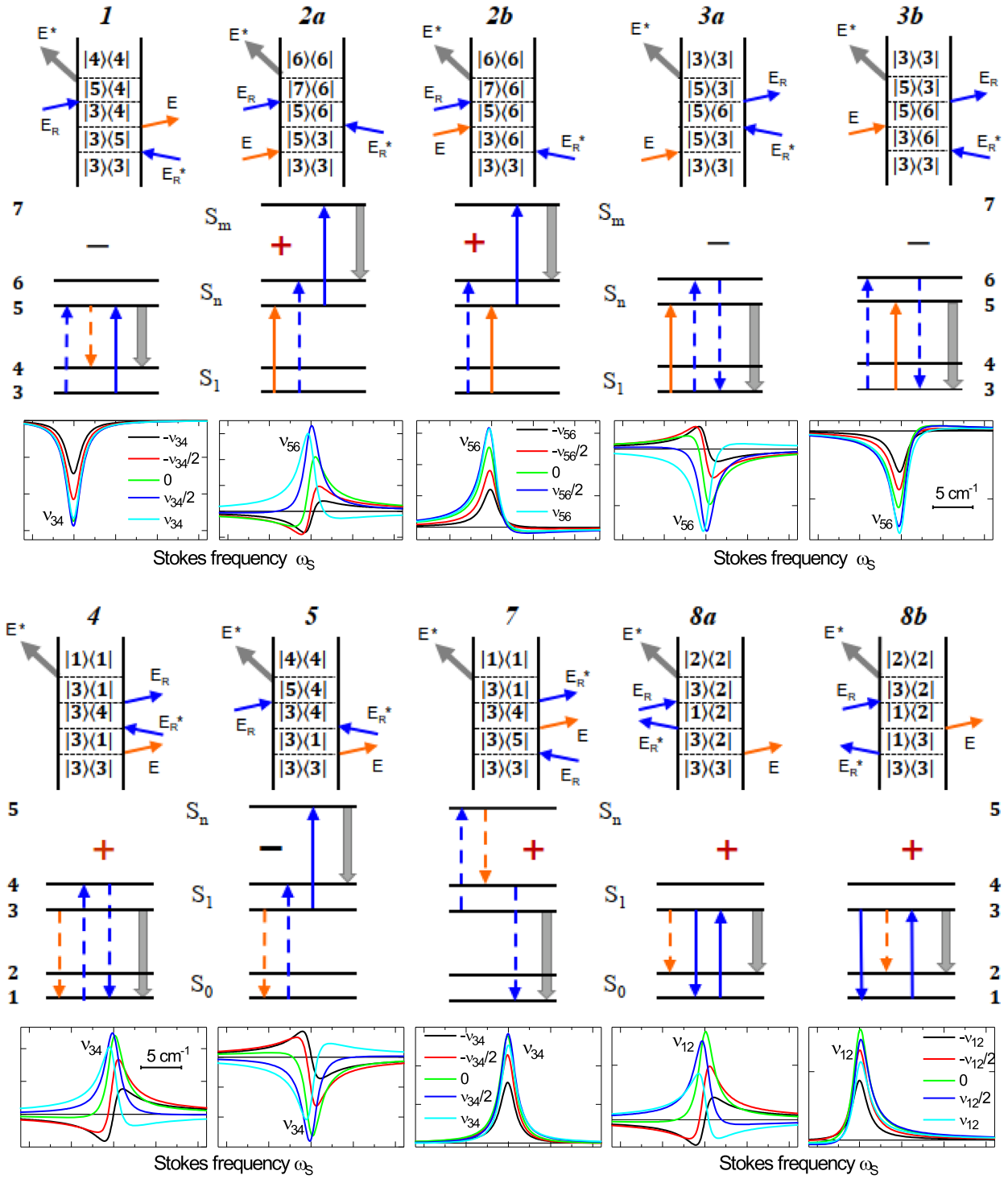

FIG. 1. Stokes FSR diagrams starting from S_1. Blue/orange arrows indicate the Raman/probe (E_R)/(E) field, with bra- (dashed) or -ket (solid) interactions. The sign $\sigma = (-1)^{N_{ket}}$ is positive for even N_{ket} (absorption) and negative for odd N_{ket} (emission). The graphs under diagrams show how the line shape changes with detuning E_R from vibronic resonance. The detuning is given in vibrational frequencies $-\nu_{ij}$, $-\nu_{ij}/2$, 0, $+\nu_{ij}/2$, and $+\nu_{ij}$, with +/− for Stokes/anti-Stokes detuning. Numerically, $\nu_{12} = 1100\ cm^{-1}$, $\nu_{34} = \nu_{56} = 900\ cm^{-1}$, $\Gamma_{13} = \Gamma_{35} = \Gamma_{57} = 200\ ps^{-1} = 1000\ cm^{-1}$, and $\Gamma_{12} = \Gamma_{34} = \Gamma_{56} = 0.2\ ps^{-1}$. For anti-Stokes diagrams and diagrams from a hot state, see the supplementary material, Figs. S3–S5 and S7–S9.

The explicit expressions for $\Delta A(\omega)$ are summarized in the Appendix.

Each term in $\Delta A(\omega)$ can be represented by a double-sided Feyn-man diagram or by an energy-level diagram as shown in Fig. 1. Here, each electronic state S_0, S_1, S_n, S_m (m > n) is associated with a pair of vibrational levels: S_0 with 1 and 2, S_1 with 3 and 4, S_n with 5 and 6, and S_m with 7. Raman E_R and probe E fields are marked by the blue and orange arrows, respectively. In the energy level diagrams, -ket/bra- is represented by a solid/dashed arrow, while in the Feynman diagrams, -ket is on the left and bra- is on the right.

Actinic excitation $S_0 \rightarrow S_1$ transfers population to level 3, which serves as the initial state for the stimulated Raman from S_1. Three successive interactions (arrows) result in the signal ΔA in Eq. (7a) given by a sum over products $\left\{ f_{mn} \cdot g_{kl} \cdot h^s_{pq} \right\}$. The first interaction h^s_{pq} leads to electronic coherence, the second g_{kl} gives vibrational coherence, and the third f_{mn} again leads to electronic coherence. h^s_{pq} enters as h^{α}_{pq} when the Raman field E_R is the first or as h^{β}_{pq} when the probe E is the first. The factor $M_{[s]}$ is the product of the transi-tion dipole moments along the path [s]. For example, for diagram 1, $M_{[1]} = \mu_{35}\mu_{54}\mu^*_{35}\mu^*_{54}$, where μ_{mn} include the vibrational overlap integral in the Condon approximation. Below, when studying the signal dependence on the Raman detuning from vibronic resonance, one can take $M_{[s]} = 1$.

Note that the diagrams contribute to the signal with a different sign $\sigma = \pm 1$, unlike in spontaneous Raman. In the spontaneous Raman, the probe E is zero and the only contributing diagram is 1 (top left), where the Raman field is absorbed to emit the Stokes probe field. To be consistent with TA spectroscopy, such a diagram must enter with a negative sign, similar to bleach or stimulated emission. This finally determines the sign σ of a diagram,[47]

$$\sigma = (-1)^{N_{ket}}. \tag{8}$$

As shown, the sign is negative for odd N_{ket} (the number of solid arrows) and positive for even N_{ket}.

Consider upper diagrams 1, 2a, 2b, 3a, and 3b in Fig. 1 reflecting $S_1 \rightarrow S_n \rightarrow S_m$ transitions from S_1 to higher states S_n and S_m (m > n). Only diagram 1 prepares coherences in S_1, while the four others deal with coherences in S_n. When the Raman field E_R is fully off-resonant, these four become negligible, and the only 1 delivers the S_1 Raman spectrum of interest. Note that the non-resonant FSR spectrum is identical to that from spontaneous Raman, as both are given by the same diagram 1.

Furthermore, when E_R becomes resonant with S_1–S_n but still non-resonant with S_n–S_m, diagrams 3a and 3b start to contribute, and the resulting Raman spectrum acquires negative bands from S_n, in addition to those from S_1. Note that these additional S_n bands can be distinguished by comparison with the non-resonant FSR spectrum (that delivers the S_1 contributions only).

When E_R is in resonance with both S_1–S_n and S_n–S_m, diagrams 2a and 2b contribute, and some Raman bands may switch their sign from negative to positive. This happens if $\mu_{nm} > \mu_{1n}$, where μ_{1n} and μ_{nm} are the corresponding transition dipole moments. In that case, the positive bands can be clearly ascribed to S_n.

Next, the actinic pump produces not only a population in S_1 but also a bleach (lack of population) in S_0. These bleach terms can be described by the same diagrams 1, 2a, 2b, 3a, and 3b, but starting from S_0 and with the opposite sign as the bleach population is negative. In the non-resonant case, the bleach term reproduces the S_0 spectra, taken with the opposite sign and scaled by the actinic population.

In the absence of actinic excitation, one starts directly from S_0. Again, diagrams 1, 2a, 2b, 3a, and 3b apply with minor modifications: S_1, S_n, and S_m are substituted with S_0, S_1, and S_n, and levels 3, 4, 5, 6, and 7 change accordingly to 1, 2, 3, 4, and 5 (see the supplementary material for details).

Now consider diagrams 4, 5, 7, 8a, and 8b in Fig. 1 reflecting the transitions to a lower electronic state S_0. Here, diagram 6 is not shown to match the numbering of Ref. 30. Far from S_0–S_1 and S_1–S_n resonances, only diagrams 4, 5, and 7 survive. The 5 and 7 are close in magnitude but opposite in sign and, therefore, cancel each other. The Raman signal results from 4 only, which is positive and associated with S_1.

To summarize the non-resonant case, the FSR signal comes from diagrams 1 and 4. Both deal with coherency in S_1 but contribute with opposite signs. The final sign of ΔA depends on the transition dipoles μ_{01} and μ_{1n} and on how far E_R is detuned from S_0–S_1 and S_1–S_n.

When E_R is in resonance with S_0–S_1, diagrams 8a and 8b contribute additional positive bands associated with S_0, as was experimentally observed by us in trans-azobenzene.[30]

Now we discuss in more detail how different diagrams behave near electronic resonances S_1–S_n, S_n–S_m, and S_0–S_1. We simulate the Raman signal with Eq. (7a) assuming $\nu_{12} = 1100\ cm^{-1}$, $\nu_{34} = \nu_{56} = 900\ cm^{-1}$, $\Gamma_v = \Gamma_{12} = \Gamma_{34} = \Gamma_{56} = 0.2\ ps^{-1}$, and $\Gamma_e = \Gamma_{13} = \Gamma_{35} = \Gamma_{57} = 200\ ps^{-1}$. The E_R detuning from the resonances was taken in units of ν_{ij}, from −1 to +1, being within the electronic bandwidth (~1000 cm^{-1}). The resulting line shapes are displayed under each diagram, always for five fixed detuning $-\nu_{ij}$, $-\nu_{ij}/2$, 0, $\nu_{ij}/2$, and ν_{ij}. As shown, when the Raman field acts first (diagrams 1, 2b, 3b, 7, and 8b), no substantial distortion of the line shape occurs. On the con-trary, when the probe is the first, the distortion is large and results in a dispersive line shape. This happens when the Raman detuning is approximately equal to the vibrational frequency. Another reason for the dispersive line shape is the simultaneous contributions with opposite signs, from higher and lower electronic states.

Previously, the dispersive line shapes were experimentally observed in stimulated Raman measurements.[6,7,16,22] Contributions from S_0 were considered by Lee and co-workers,[10–13] while the S_n contributions and the dependence on resonance conditions were discussed by Oscar *et al.*,[17] although without specifying the sign of the contributing terms.

The above consideration implies that only level 3 is initially populated by an actinic pump. However, for low-frequency modes, level 4 can be populated as well, which doubles the number of contributing diagrams (see Figs. S4, S5, S8, and S9 for hot Stokes and anti-Stokes diagrams). For example, diagram 4 of Fig. 1 would have a counterpart given by diagram 4 of Fig. S8. It follows that the latter contributes with the same positive sign, leaving the total signal (the sum from levels 3 and 4) to be the same as the full population would be at level 3.

IV. QUANTUM CHEMICAL COMPUTATIONS

The ground and excited state Raman spectra are calculated at the density functional theory (DFT) and the linear response time-dependent DFT (TDDFT), respectively, with the use of the Firefl

software.[55] The PBE0 hybrid exchange–correlation functional and the Def2-TZVPP basis set were used. The spectra are calculated in the standard non-resonant approximation. To our experience with related stilbene compounds, the inclusion of the resonant effects via the pre-resonance methodology rarely delivers a decisive improvement; furthermore, such an approach is hardly feasible for the excited states. The calculated harmonic frequencies were scaled by a factor of 0.962 to achieve better correspondence with the experiment, as is common practice.[60]

V. EXPERIMENTAL

Our TA and FSR setups are described in great detail elsewhere.[28–31,56–59]

For TA,[56–59] 30 fs pulses at 800 nm, 500 Hz are converted to 400 nm and then pass through a 1 mm CaF_2 to generate a broadband continuum probe in the range 275–700 nm. The probe is split into signal and reference and registered with two polychromators. Fifty-fs pump pulses are derived from an optical parametric amplifier in the range 270–900 nm. The sample flows through a measurement cell of 0.3 mm thickness with fused silica windows of 0.2 mm. The pump and probe are focused to a ~0.15 mm spot in the cell and inter-sect at ~15°. The pump is chopped to block every second pulse to record the baseline. The TA spectra $\Delta A(\lambda, t)$ are measured with par-allel, perpendicular, and magic angle polarization. Multiple (10–40) back and forth pump–probe scans are applied to improve signal-to-noise. The spectra at negative delays are subtracted to eliminate pump scattering and sample fluorescence.

For FSR,[28–31] the general scheme is basically similar to TA, with a ~2-ps Raman pump added in boxcar geometry. Thirty-fs actinic pump and probe are derived from noncollinear optical paramet-ric amplifiers (NOPAs).[28] The probe pulse of 1000 cm^{-1} width is used directly without continuum generation. The Raman pump is chopped, and thus, the actinic pump is included in the baseline. The Raman spectra at negative delays are subtracted to eliminate the solvent and ground-state contributions.[28]

VI. S_0 RAMAN SPECTRA

Ground-state Stokes Raman spectra are shown in Fig. 2. These are recorded without actinic excitation, with the Raman pump at 645 or 621 nm, far from the stationary absorption band at ~330 nm. In this strongly non-resonant case, only diagram 1 contributes to the stimulated Raman, and as discussed above, the FSR spectra reproduce those from the stationary spontaneous Raman.

The low-frequency region <800 cm^{-1} is dominated by bend-ing and deformation modes with low Raman activity, very similar to stilbene. The activity in the low-frequency range strongly increases from tt- to ct- and further to cc-isomer, reflecting the lower rigidity of the cis-conjugation. The two most intense lines are located around 1600 cm^{-1} and correspond to C–C– and C=C– stretching modes.

VII. EXCITED-STATE SPECTRA

Stokes Raman spectra from S_1, under actinic excitation of tt, ct, and cc, are presented in Fig. 3 (right). Here, the computed spectra are also shown by vertical bars. The experimental spectra reveal mainly negative bands from vibrational coherences in S_1 or S_n. A band at 580 cm^{-1} is positive, which may indicate a resonance between E_R

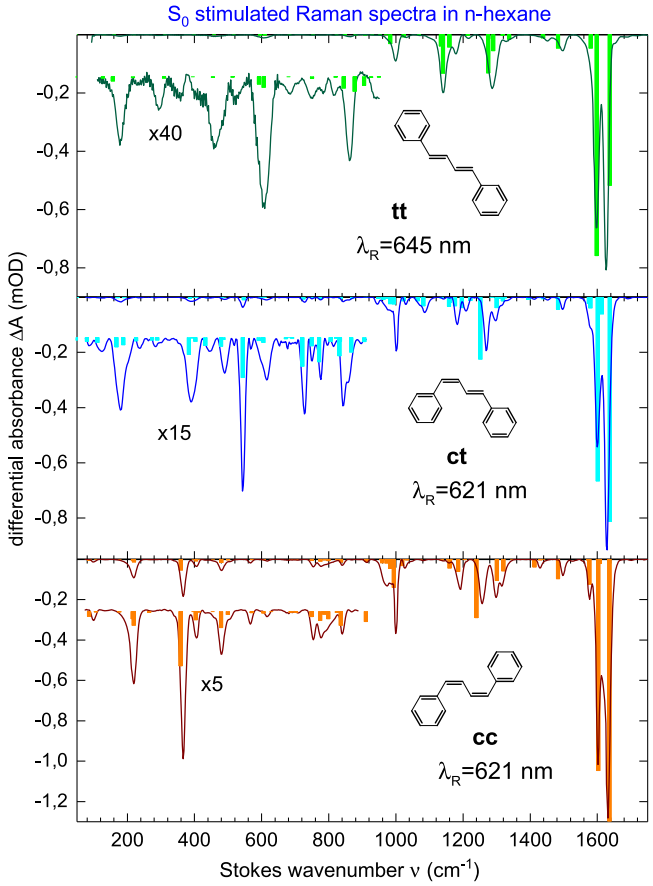

FIG. 2. S_0 Stokes FSR spectra of tt, ct, and cc DPB in n-hexane, without actinic excitation, with the Raman pump at λ_R = 645 nm for tt and λ_R = 621 nm for ct and cc. Theoretically computed spectra are given by vertical bars.

and $S_n \rightarrow S_m$ (diagrams 2a and 2b). We shall discuss this point in Sec. VIII. Here, we briefly discuss the TA spectra at the left of Fig. 3.[59]

For tt (top), the TA spectra reveal three well-separated regions: negative bleach about 300 nm, negative stimulated emission (SE) at 400 nm, and positive excited-state absorption (ESA) at 650 nm associated with an $S_1 \rightarrow S_n$ transition. The TA decay with ~500 ps is mainly due to photoisomerization tt → ct.[59] For ct (middle), the gen-eral evolution looks similar. The ESA is nearly the same, while the SE band is slightly red-shifted, and the ct decay occurs with ~20 ps, reflecting faster photoisomerization ct → tt. Finally for cc (bottom), the ESA band shifts a bit more to the red, and the SE is too weak to be observed, while instead the *P*-band (of perpendicular molecu-lar configuration)[59] at 400 nm appears at early time t = 0.3 ps. The cc → ct photoisomerization proceeds even faster, with 6 ps.[59]

The optimized geometry of the DPB molecule and the electronic structure of the S_0 and S_1 states have been reported in Ref. 59. The solution-phase S_1 is due to a single-electron excitation from the HOMO to the LUMO and is, therefore, correctly describable by TDDFT. Contrariwise, the gas-phase S_1 includes a considerable contribution of the double excitation, and in a non-polar solution, the two states will remain rather close to each other. Therefore, one

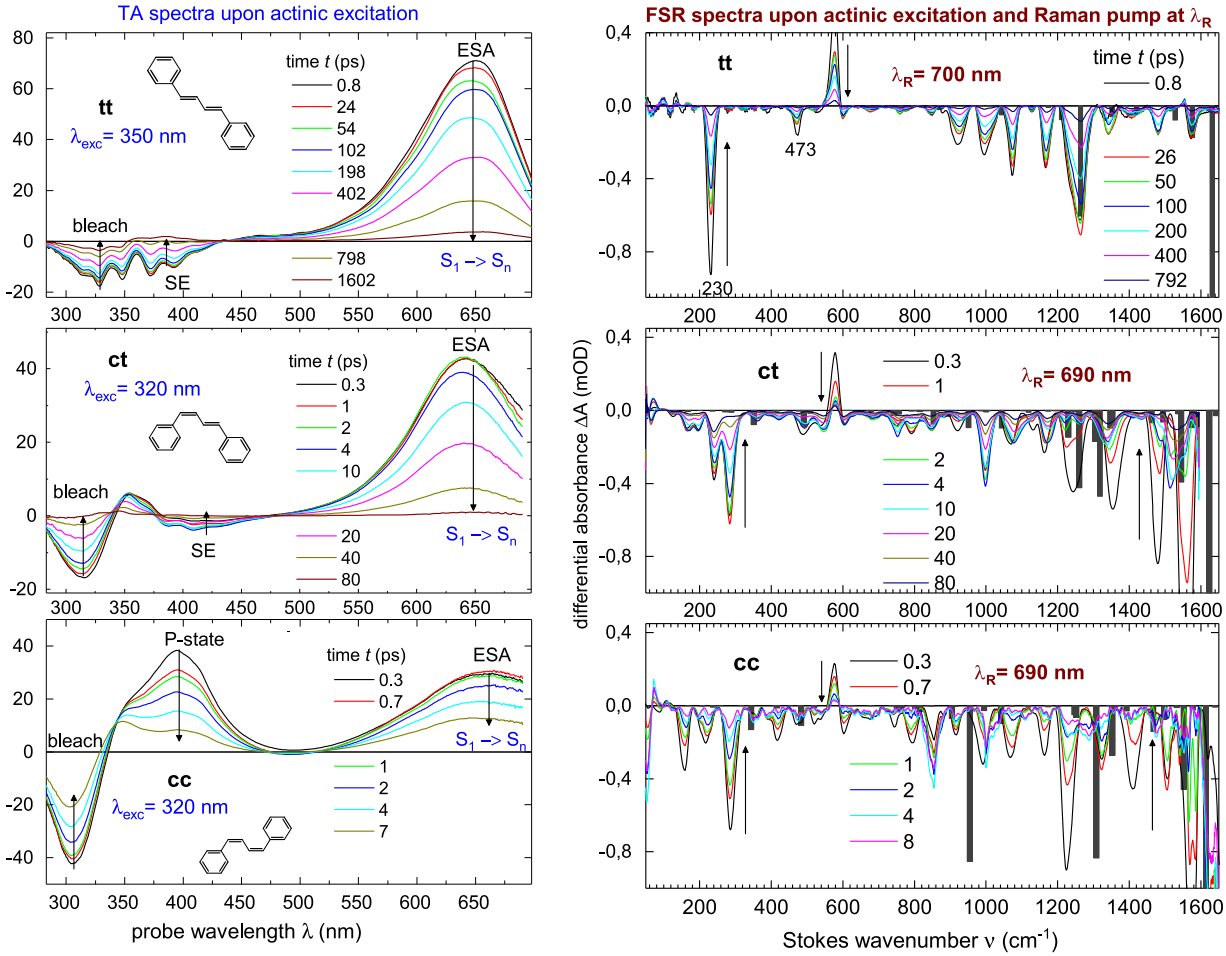

FIG. 3. TA spectra[59] (left) and Stokes FSR spectra (right) of tt, ct, and cc DPB in n-hexane upon $S_0 \rightarrow S_1$ actinic excitation, λ_{ac} = 320–350 nm, with the Raman pump at λ_R = 690–700 nm. The computed Raman spectra are displayed by vertical bars. Vertical arrows indicate the signal evolution.

cannot confidently rule out some involvement of the doubly excited state via, e.g., its partial thermal population. A quantitatively reliable description of those subtle effects of solvent-dependent state reordering in DPB, perhaps, needs more accurate experimental data to calibrate the computational results against. One more complication may arise from the very short lifetime of the excited cc-isomer. Its Raman signal may correspond to some ensemble of configurations along its photoisomerization pathway, which is not entirely accessible by TDDFT due to diminishing the S_0–S_1 gap upon the cc → ct twisting.

As one can see that, while the ground-state calculations reproduce the major spectral bands (see Fig. 2) rather well, the excited state data in Fig. 3 show less satisfactory agreement. Possibly, the discrepancies in the cc and ct isomers are rather quantitative than qualitative, and the major calculated bands are just unevenly displaced from the experimental ones. Perhaps, those discrepancies could be refined by a costly higher-level calculation of vibrational frequencies. Surprisingly, the tt-isomer whose excited-state lifetime is, conveniently, the longest and seems to pose a more important problem: it lacks highly intense bands around 1600 cm^{-1}. Those bands are due to the symmetric stretching vibrations in the conjugated system, and our calculations predict them, rather expectedly, to dominate in all isomers both in the ground and in the excited state. One can hypothesize that here we indeed observe some resonant effects that result from non-trivial couplings with the respective S_n manifold.

VIII. EFFECT OF $S_n \rightarrow S_m$ RESONANCE

The Raman pump E_R at 690–700 nm hits the ESA band in resonance with the S_1–S_n transition and is far from the $S_1 \rightarrow S_0$ resonance. Hence, the lower diagrams 4, 5, 7, 8a, and 8b are strongly suppressed and can be neglected. Among the rest, diagram 1 brings a contribution from vibrational coherences in S_1, while 2a, 2b, 3a, and 3b deliver the signals from coherences in S_n. The positive signal may appear from 2a and 2b when E_R is in resonance with $S_n \rightarrow S_m$.

The position of the $S_n \rightarrow S_m$ band can be established in a double-pump experiment, $S_0 \rightarrow S_1 \rightarrow S_n$, when the $S_0 \rightarrow S_1$ excitation

is followed by a delayed $S_1 \rightarrow S_n$ excitation. Here, the first pulse populates S_1, while the second, after a 1 ps delay, transfers the population further to S_n. The first pump pulse is not chopped and is included in the baseline, the pump–probe delay t being countered from the second pulse. The resulting TA spectra are presented in Fig. 4.

The $S_n \rightarrow S_m$ absorption band can be restored by subtracting the early bleach at t = 0.08 ps from the top spectra. The bleach shape is given by the ESA band in Fig. 3 (top left), and its ampli-tude is adjusted to get approximately zero signal at t = 0.08 ps at the band peak (a nearly zero signal is expected upon subtraction as the bleach dominates in that range). The resulting spectra are displayed at the bottom of Fig. 4. It is shown that the S_n–S_m band is peaked at 560 nm, and the Raman pump at 700 nm hits its absorption edge only. One hardly expects a large positive Raman signal at such conditions; however, it should increase when the Raman pump is tuned closer to the S_n–S_m peak. We, therefore, perform FSR measurements with tunable Raman pump E_R in the range λ_R = 645–700 nm.

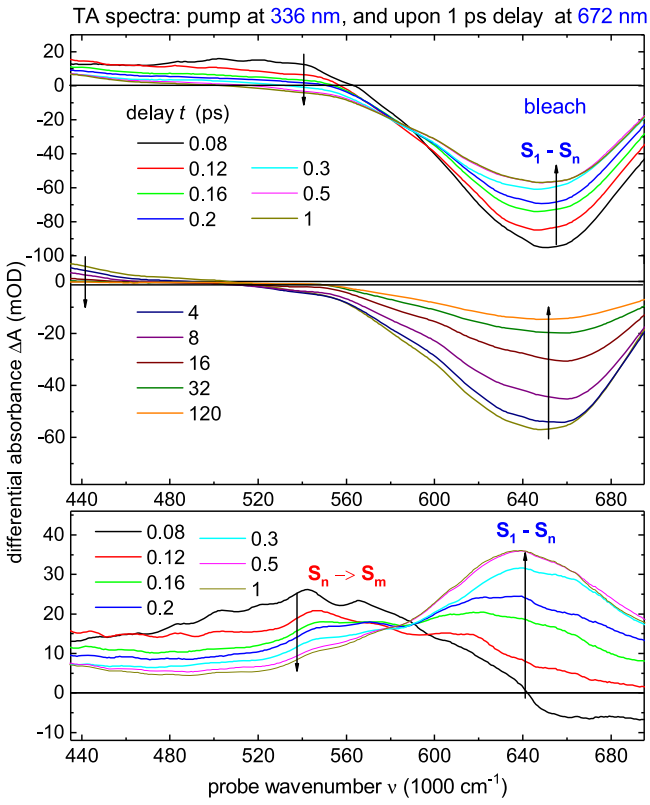

FIG. 4. (Top) TA spectra of tt in n-hexane upon double excitation $S_0 \rightarrow S_1 \rightarrow S_n$ at 336 and 672 nm with a 1 ps delay. The first pump is not chopped and included in the baseline. Delay t is countered from the second pump. The initial bleach reflect $S_1 \rightarrow S_n$ population transfer, followed by $S_n \rightarrow S_1$ conversion with ~0.1 ps (on top) and subsequent cooling in S_1 with ~10 ps (middle). The residual bleach at 120 ps indicates a lack of population in S_1 since some S_n population does not return back to S_1. (Bottom) The spectra up to 1 ps upon subtracting the bleach. The bleach is given by negative ESA (Fig. 3, top left) whose amplitude is adjusted to get a zero signal at t = 0.08 ps at the ESA peak. The resulting spectra reveal the $S_n \rightarrow S_m$ band of interest.

The top frame in Fig. 5 shows the FSR spectra of tt in n-hexane recorded under these conditions. One sees that a band at 225 cm^{-1} switches its sign from negative to positive when E_R shifts to the blue, closer to the $S_n \rightarrow S_m$ resonance. Other bands at 142, 471, and 581 cm^{-1} behave similarly although without switching their sign. Such behavior qualitatively agrees with an increasing contribution from diagrams 2a and 2b, and therefore, the bands can be ascribed to S_n. As already mentioned, the S_n bands should disappear when tun-ing the Raman pump far to the red. Unfortunately, the non-resonant case cannot be realized in our setup.

The bottom frame of Fig. 5 displays our simulations, using Eq. (7a) or Eqs. (A1)–(A3) of the Appendix, with the S_n lifetime τ = 0.1 ps, and $\Gamma_{35} = \Gamma_{57}$ = 200 ps^{-1} and Γ_{56} = 0.2 ps^{-1}. Note that τ = 0.1 ps corresponds to the spectral width (FWHM) of 56 cm^{-1}. The simulated spectra generally well reproduce the experimental features but differ by long red tails of the bands, not seen in the experiment. These tails originate mainly from broadening due to shortly lived S_n and partly from the exponential pulses. In the experimental spectra, the tails may be hidden under a complicated Raman background (see Fig. S10, top), which has to be subtracted to get background-free Raman spectra.

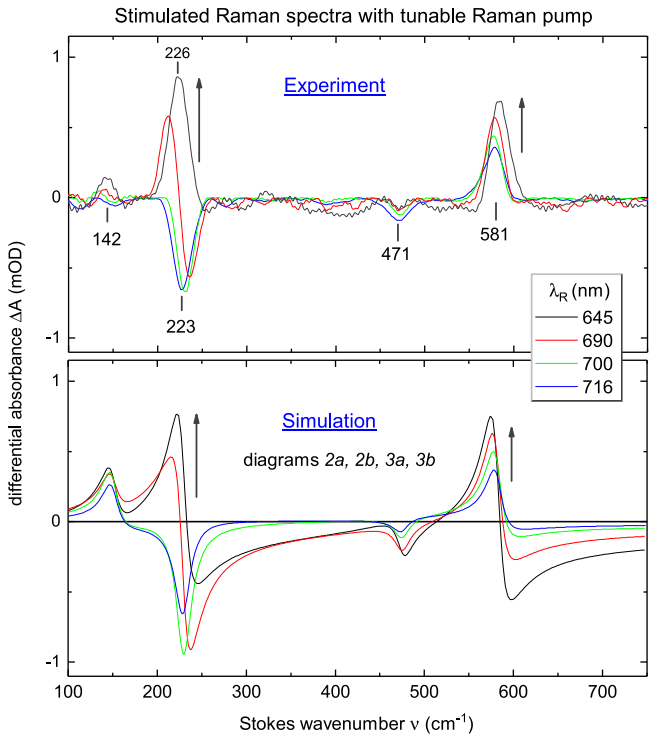

FIG. 5. (Top) FSR spectra of tt in n-hexane upon $S_0 \rightarrow S_1$ actinic excitation, with the Raman pump at 645, 690, 700, and 716 nm, reveal four bands at 142, 225, 471, and 581 cm^{-1}, which develop from negative to positive when approaching the $S_n \rightarrow S_m$ resonance, reflecting an increasing contribution from diagrams 2a and 2b. (Bottom) Simulated spectra by Eq. (7a), with diagrams 2a, 2b, 3a, and 3b and with S_n lifetime τ = 0.1 ps, and $\Gamma_{35} = \Gamma_{57}$ = 200 ps^{-1} and Γ_{56} = 0.2 ps^{-1}. The simulated spectra generally agree with the experimental ones; the difference is in the long red tails due to broadening by short τ = 0.1 ps that corresponds to the width (FWHM) of 56 cm^{-1}.

IX. CONCLUSION

We have analytically calculated the FSR signal and its line shape upon $S_0 \rightarrow S_1$ actinic excitation at different detuning of the Raman pump from higher ($S_1 \rightarrow S_n \rightarrow S_m$) and lower ($S_1 \rightarrow S_0$) electronic resonances. Generally, the signal includes 15 Feynman diagrams. Unlike spontaneous Raman, the FSR signal contains contributions of different signs, resulting in a net positive or negative signal or producing a dispersive line shape that strongly depends on the resonance conditions.

In the case of the $S_1 \rightarrow S_n$ resonance only, the Stokes Raman spectra are negative and originate both from S_1 and S_n vibrational coherencies. The S_n coherences will disappear in the non-resonance case, and, thus, they can be distinguished from the coherences in S_1. When the $S_n \rightarrow S_m$ resonance starts to contribute, some Raman bands may switch their sign from negative to positive.

If $S_1 \rightarrow S_0$ is also in resonance, the spectra reveal positive bands from S_0. The spectra, recorded with different Raman detuning from the electronic resonances, agree qualitatively with analytically simulated spectra.

We pay attention to the deep connection between transient absorption and stimulated Raman spectroscopy. When higher electronic resonances $S_1 \rightarrow S_n \rightarrow S_m$ contribute to the resonance Raman signal, the relevant information on the excited states can be obtained from the TA measurements.

In addition, the Raman spectra of tt-, ct-, and cc-isomers of diphenylbutadiene are measured for the first time, and the S_0 spectra are in reasonable agreement with theoretically computed spectra.

SUPPLEMENTARY MATERIAL

The supplementary material includes a detailed theoretical description of the stimulated Raman signal; the Stokes and anti-Stokes diagrams from ground S_0 and excited S_1 and S_n electronic states, for cold and hot vibrational states; and the computed Raman frequencies for three isomers of diphenylbutadiene.

ACKNOWLEDGMENTS

O.A.K. acknowledges the National Science Foundation for support under Grant No. CHE 1900226. The computations were carried out using the facilities of HPC computing resources at Lomonosov Moscow State University.

AUTHOR DECLARATIONS

Conflict of Interest

The authors have no conflict to disclose.

DATA AVAILABILITY

The data that support the findings of this study are available from the corresponding authors upon reasonable request.

APPENDIX: CALCULATING STIMULATED RAMAN SIGNAL

A compact form of the Raman signal is obtained by taking the imaginary part in Eqs. (7a) and (7b). The Raman signal can be presented as the product (A3) of three Lorentzians multiplied by a second-order polynomial $\Phi(x_e)$. Lorentzians $L_{mn}(x_e)$, $L^{\alpha}_{pq}(x_e)$, and $L^{\beta}_{pq}(x_e)$ are determined by the electronic resonance conditions; the vibrational coherence gives rise to the Lorentzian $L_{kl}(\omega_v)$, where ω_v is the vibrational frequency. Depending on the roots of the polynomial, the Raman signal may change sign. If the polynomial passes through zero at the resonance frequency ω_v, the band is dispersive with negative and positive wings. The FSR signal can be expressed as

$$F_{\alpha}(mn,kl,pq) = \sigma \cdot \frac{a_{\alpha}{\omega_s}^2 + b_{\alpha}\omega_s + c_{\alpha}}{\left[(\omega_s + x_{mn})^2 + \Gamma_e^2\right]\left[(\omega_s + \omega_v)^2 + \Gamma_v^2\right]\left[{x^{\alpha}_{pq}}^2 + \Gamma_e^2\right]}, \tag{A1}$$

$$F_{\beta}(mn,kl,pq) = \sigma \cdot \frac{a_{\beta}{\omega_s}^2 + b_{\beta}\omega_s + c_{\beta}}{\left[(\omega_s + x_{mn})^2 + \Gamma_e^2\right]\left[(\omega_s + \omega_v)^2 + \Gamma_v^2\right]\left[\left(\omega_s + x^{\beta}_{pq}\right)^2 + \Gamma_e^2\right]}, \tag{A2}$$

$$F_{\alpha,\beta}(mn,kl,pq) = \sigma \cdot \Phi(x_e) \cdot L_{mn}(x_e) \cdot L_{kl}(\omega_v) \cdot L^{\alpha,\beta}_{pq}(x_e), \tag{A3}$$

$$\Phi(x_e) = \Phi\left(x_{mn}, x^{\alpha,\beta}_{pq}\right) = a_{\alpha,\beta}{\omega_s}^2 + b_{\alpha,\beta}\omega_s + c_{\alpha,\beta}, \tag{A4}$$

$$L_{mn}(x_e) = \frac{\Gamma_e^2}{(\omega_s + x_{mn})^2 + \Gamma_e^2}, \tag{A5}$$

$$L^{\alpha}_{pq}(x_e) = \frac{\Gamma_e^2}{\left(x^{\alpha}_{pq}\right)^2 + \Gamma_e^2}, \quad L^{\beta}_{pq}(x_e) = \frac{\Gamma_e^2}{\left(\omega_s + x^{\beta}_{pq}\right)^2 + \Gamma_e^2}, \tag{A6}$$

$$L_{kl}(\omega_v) = \frac{\Gamma_v^2}{(\omega_s + \omega_v)^2 + \Gamma_v^2}, \tag{A7}$$

$$a_{\alpha} = \Gamma_e, \quad b_{\alpha} = \Gamma_e\left(x_{mn} + \omega_v - x^{\alpha}_{pq}\right) - \Gamma_v x^{\alpha}_{pq}, \tag{A8}$$

$$c_{1\alpha} = -\Gamma_e^2\Gamma_v + \Gamma_e\omega_v\left(x_{mn} - x^{\alpha}_{pq}\right) - \Gamma_v x_{mn} x^{\alpha}_{pq}, \tag{A9}$$

$$a_{\beta} = 2\Gamma_e + \Gamma_v, \quad b_{\beta} = \Gamma_e\left(x_{mn} + 2\omega_v + x^{\beta}_{pq}\right) + \Gamma_v\left(x_{mn} + x^{\beta}_{pq}\right), \tag{A10}$$

$$c_{\beta} = -\Gamma_e^2\Gamma_v + \Gamma_e\omega_v\left(x_{mn} + x^{\beta}_{pq}\right) + \Gamma_v x_{mn} x^{\beta}_{pq}, \tag{A11}$$

$$x^{\alpha,\beta}_{pq} = (\Omega_R \pm \omega_{pq}), \quad x_{mn} = (\Omega_R - \omega_{mn}), \quad \omega_s = (\omega - \Omega_R), \tag{A12}$$

$$\Gamma_e = \Gamma_{mn} = \Gamma_{pq}, \quad \Gamma_v = \Gamma_{kl}. \tag{A13}$$

Here, ω_s is the detuning from Ω_R, ω_v is the vibrational frequency, and Γ_{ij} is the half width at half maximum. The FRS signal is given by

the sum over all pathways [s] through the vibrational manifolds in S_0, S_1, and S_n.

The potential energy for the electronic states is assumed to be separable into normal harmonic modes with frequencies ν_j along intramolecular coordinates q_j. The relative geometry of S_n/S_m is taken to be identical to S_0/S_1 for simplicity. All vibronic transitions are organized in Franck–Condon progressions. Within the Born–Oppenheimer approximation, $\mu_{ab} = \mu_{ab}^{el} \times \langle a|b\rangle$, where μ_{ab}^{el} is the electronic transition dipole operator and $\langle a|b\rangle$ is the vibrational overlap integral, with its square equals the Franck–Condon factors $|\langle n|k\rangle|^2$.

REFERENCES

[1]M. Yoshizawa and M. Kurosawa, "Femtosecond time-resolved Raman spectroscopy using stimulated Raman scattering," Phys. Rev. A **61**, 013808 (1999). [2]D. R. Dietze and R. A. Mathies, "Femtosecond stimulated Raman spectroscopy," ChemPhysChem **17**, 1224–1251 (2016).

[3]P. Kukura, D. W. McCamant, P. H. Davis, and R. A. Mathies, "Vibrational structure of the S_2 ($1B_u$) excited state of diphenyloctatetraene observed by femtosecond stimulated Raman spectroscopy," Chem. Phys. Lett. **382**, 81–86 (2003).

[4]S.-Y. Lee, D. Zhang, D. W. McCamant, P. Kukura, and R. A. Mathies, "Theory of femtosecond stimulated Raman spectroscopy," J. Chem. Phys. **121**, 3632–3642 (2004).

[5]P. Kukura, D. W. McCamant, S. Yoon, D. B. Wandschneider, and R. A. Mathies, "Structural observation in vision with femtosecond-stimulated Raman," Science **310**, 1006–1009 (2005).

[6]P. Kukura, D. W. McCamant, and R. A. Mathies, "Femtosecond stimulated Raman spectroscopy," Annu. Rev. Phys. Chem. **58**, 461–488 (2007).

[7]R. R. Frontiera, S. Shim, and R. A. Mathies, "Origin of negative and dispersive features in anti-Stokes and resonance femtosecond stimulated Raman spectroscopy," J. Chem. Phys. **129**, 064507 (2008).

[8]C. Fang, R. R. Frontiera, R. Tran, and R. A. Mathies, "Mapping GFP structure evolution during proton transfer with femtosecond Raman spectroscopy," Nature **462**, 200–205 (2009).

[9]S. R. Ellis, D. P. Hoffman, M. Park, and R. A. Mathies, "Difference bands in time-resolved femtosecond stimulated Raman spectra of photoexcited intermolecular electron transfer from chloronaphthalene to tetracyanoethylene," J. Phys. Chem. A **122**, 3594–3605 (2018).

[10]Z. Sun, J. Lu, D. H. Zhang, and S.-Y. Lee, "Quantum theory of femtosecond time-resolved stimulated Raman scattering," J. Chem. Phys. **128**, 144114 (2008).

[11]K. Niu, S. Cong, and S.-Y. Lee, "Femtosecond stimulated Raman scattering for polyatomics with harmonic potential," J. Chem. Phys. **131**, 054311 (2009).

[12]K. Niu, B. Zhao, Z. Sun, and S.-Y. Lee, "Analysis of femtosecond stimulated Raman spectroscopy of excited-state evolution in bacteriorhodopsin," J. Chem. Phys. **132**, 084510 (2010).

[13]K. Niu and S.-Y. Lee, "Analysis of time resolved femtosecond/picosecond coherent anti-Stokes Raman spectroscopy: Application to toluene and rhodamine 6G," J. Chem. Phys. **136**, 064504 (2012).

[14]J. M. Rhinehart, J. R. Challa, and D. W. McCamant, "Multimode charge-transfer dynamics of 4-(dimethylamino)benzonitrile probed with ultraviolet femtosecond stimulated Raman spectroscopy," J. Phys. Chem. B **116**, 10522–10534 (2012). [15]J. Lee, J. R. Challa, and D. W. McCamant, "Ultraviolet light makes dGMP floppy: Femtosecond stimulated Raman spectroscopy of 2′-deoxyguanosine 5′-monophosphate," J. Phys. Chem. B **121**, 4722–4732 (2017).

[16]W. Liu, F. Han, C. Smith, and C. Fang, "Ultrafast conformational dynamics of pyranine during excited state proton transfer in aqueous solution revealed by femtosecond stimulated Raman spectroscopy," J. Phys. Chem. B **116**, 10535–10550 (2012).

[17]B. G. Oscar, C. Chen, W. Liu, L. Zhu, and C. Fang, "Dynamic Raman line shapes on an evolving excited-state landscape: Insights from tunable femtosecond stimulated Raman spectroscopy," J. Phys. Chem. A **121**, 5428–5441 (2017).

[18]C. Fang, L. Tang, B. G. Oscar, and C. Chen, "Capturing structural snapshots during photochemical reactions with ultrafast Raman spectroscopy: From materials transformation to biosensor responses," J. Phys. Chem. Lett. **9**, 3253–3263 (2018).

[19]R. R. Frontiera, A.-I. Henry, N. L. Gruenke, and R. P. Van Duyne, "Surface-enhanced femtosecond stimulated Raman spectroscopy," J. Phys. Chem. Lett. **2**, 1199–1203 (2011).

[20]S. M. Hart, W. R. Silva, and R. R. Frontiera, "Femtosecond stimulated Raman evidence for charge-transfer character in pentacene singlet fission," Chem. Sci. **9**, 1242–1250 (2018).

[21]A. A. Cassabaum, K. Bera, C. C. Rich, B. R. Nebgen, S. Y. Kwang, M. L. Clapham, and R. R. Frontiera, "Femtosecond stimulated Raman spectro-microscopy for probing chemical reaction dynamics in solid-state materials," J. Chem. Phys. **153**, 030901 (2020).

[22]S. Umapathy, B. Mallick, and A. Lakshmanna, "Mode-dependent dispersion in Raman line shapes: Observation and implication from ultrafast Raman loss spectroscopy," J. Chem. Phys. **133**, 024505 (2010).

[23]S. Mukamel and J. D. Biggs, "Communication: Comment on the effective temporal and spectral resolution of impulsive stimulated Raman signals," J. Chem. Phys. **134**, 161101 (2011).

[24]K. E. Dorfman, B. P. Fingerhut, and S. Mukamel, "Time-resolved broadband Raman spectroscopies: A unified six-wave-mixing representation," J. Chem. Phys. **139**, 124113 (2013).

[25]Q. Cen, Y. He, M. Xu, J. Wang, and Z. Wang, "Wavelength dependent resonance Raman band intensity of broadband stimulated Raman spectroscopy of malachite green in ethanol," J. Chem. Phys. **142**, 114201 (2015).

[26]G. Batignani, G. Fumero, E. Pontecorvo, C. Ferrante, S. Mukamel, and T. Scopigno, "Genuine dynamics vs cross phase modulation artifacts in femtosecond stimulated Raman spectroscopy," ACS Photonics **6**, 492–500 (2019).

[27]A. Weigel, A. Dobryakov, B. Klaumünzer, M. Sajadi, P. Saalfrank, and N. P. Ernsting, "Femtosecond stimulated Raman spectroscopy of flavin after optical excitation," J. Phys. Chem. B **115**, 3656–3680 (2011).

[28]S. A. Kovalenko, A. L. Dobryakov, and N. P. Ernsting, "An efficient setup for femtosecond stimulated Raman spectroscopy," Rev. Sci. Instum. **82**, 063102 (2011).

[29]A. L. Dobryakov, I. Ioffe, A. A. Granovsky, N. P. Ernsting, and S. A. Kovalenko, "Femtosecond Raman spectra of *cis*-stilbene and *trans*-stilbene with isotopomers in solution," J. Chem. Phys. **137**, 244505 (2012).

[30]A. L. Dobryakov, M. Quick, I. N. Ioffe, A. A. Granovsky, N. P. Ernsting, and S. A. Kovalenko, "Excited-state Raman spectroscopy with and without actinic excitation: S_1 Raman spectra of trans-azobenzene," J. Chem. Phys. **140**, 184310 (2014).

[31]M. Quick, A. L. Dobryakov, S. A. Kovalenko, and N. P. Ernsting, "Resonance femtosecond stimulated Raman spectroscopy without actinic excitation showing low-frequency vibrational activity in the S_2 state of all-trans β-carotene," J. Phys. Chem. Lett. **6**, 1216–1220 (2015).

[32]E. Pontecorvo, C. Ferrante, C. G. Elles, and T. Scopigno, "Structural rearrangement accompanying the ultrafast electrocyclization reaction of a photochromic molecular switch," J. Phys. Chem. B **118**, 6915–6921 (2014).

[33]G. Batignani, E. Pontecorvo, C. Ferrante, M. Aschi, C. G. Elles, and T. Scopigno, "Visualizing excited-state dynamics of a diaryl thiophene: Femtosecond stimulated Raman scattering as a probe of conjugated molecules," J. Phys. Chem. Lett. **7**, 2981–2988 (2016).

[34]T. J. Quincy, M. S. Barclay, M. Caricato, and C. G. Elles, "Probing dynamics in higher-lying electronic states with resonance-enhanced femtosecond stimulated Raman spectroscopy," J. Phys. Chem. A **122**(42), 8308–8319 (2018).

[35]M. S. Barclay, M. Caricato, and C. G. Elles, "Femtosecond stimulated Raman scattering from triplet electronic states: Experimental and theoretical study of resonance enhancements," J. Phys. Chem. A **123**, 7720–7732 (2019).

[36]M. Pižl, A. Picchiotti, M. Rebarz, N. Lenngren, L. Yingliang, S. Záliš, M. Kloz, and A. Vlček, "Time-resolved femtosecond stimulated Raman spectra and DFT anharmonic vibrational analysis of an electronically excited rhenium photosensitizer," J. Phys. Chem. A **124**, 1253–1265 (2020).

[37]K. Iwata and H.-o. Hamaguchi, "Picosecond structural relaxation of S_1 trans-stilbene in solution as revealed by time-resolved Raman spectroscopy," Chem. Phys. Lett. **196**, 462–468 (1992).

[38]B. M. Pierce and R. R. Birge, "A theoretical study of the low-frequency normal modes of all-trans-1,4-diphenyl-1,3-butadiene," J. Phys. Chem. **86**, 2651–2656 (1982).

[39]R. Wilbrandt, N.-H. Jensen, and F. W. Langkilde, "Time-resolved resonance Raman spectrum of all-trans-diphenylbutadiene in the lowest excited singlet state," Chem. Phys. Lett. **111**, 123–127 (1984).

[40]T. L. Gustafson, J. F. Palmer, and D. M. Roberts, "The structure of S_1 diphenylbutadiene: UV resonance Raman and picosecond transient Raman studies," Chem. Phys. Lett. **127**, 505–511 (1986).

[41]D. L. Morris, Jr. and T. L. Gustafson, "Solvent/solute interactions probed by picosecond transient Raman spectroscopy: S_1 1,4-diphenyl-1,3-butadiene in the linear alkanes," Appl. Phys. B **59**, 389–395 (1994).

[42]D. L. Morris, Jr. and T. L. Gustafson, "Solvent/solute interactions probed by picosecond transient Raman spectroscopy: Vibrational dynamics and state ordering in S1 1,4-diphenyl-1,3-butadiene," J. Phys. Chem. **98**, 6725–6730 (1994).

[43]T. Kamisuki and C. Hirose, "Transient resonance CARS and CSRS of diphenylbutadiene-d_4 in the S_0, S_1, T_1 and photoinduced radical ion states," J. Raman Spectrosc. **25**, 307–311 (1994).

[44]J. D. Leonard, Jr. and T. L. Gustafson, "The 211 nm excited resonance Raman spectra of trans-stilbene and related molecules," J. Mol. Struct. **379**, 109–120 (1996).

[45]J. Oberlé, E. Abraham, A. Ivanov, G. Jonusauskas, and C. Rullière, "Picosecond photoinduced formation of a radical cation: CARS and transient absorption studies of 1,4-diphenylbutadiene," J. Photochem. Photobiol., A **105**, 217–223 (1997).

[46]Z. A. E. Waller, R. D. Bowen, and H. G. M. Edwards, "Raman spectroscopic and structural investigation of 1,4-diphenylbutadiene and selected monomethyl and dimethyl substituted homologues," Anal. Chim. Acta **580**, 47–54 (2006).

[47]S. Mukamel, *Principles of Nonlinear Optical Spectroscopy* (Oxford University Press, 1995).

[48]S. Mukamel, "Stochastic theory of resonance Raman line shapes of polyatomic molecules in condensed phases," J. Chem. Phys. **82**, 5398–5408 (1985).

[49]Y. J. Yan and S. Mukamel, "Femtosecond pump-probe spectroscopy of polyatomic molecules in condensed phases," Phys. Rev. A **41**, 6485–6504 (1990).

[50]S. Mukamel, "Femtosecond optical spectroscopy," Annu. Rev. Phys. Chem. **41**, 647–681 (1990).

[51]R. F. Loring, Y. J. Yan, and S. Mukamel, "Time-resolved fluorescence and hole-burning line shapes of solvated molecules: Longitudinal dielectric relaxation and vibrational dynamics," J. Chem. Phys. **87**, 5840–5857 (1987).

[52]Y. J. Yan, L. E. Fried, and S. Mukamel, "Ultrafast pump-probe spectroscopy: Femtosecond dynamics in Liouville space," J. Phys. Chem. **93**, 8149–8162 (1989).

[53]A. L. Dobryakov, S. A. Kovalenko, and N. P. Ernsting, "Coherent and sequential contributions to femtosecond transient absorption spectra of a rhodamine dye in solution," J. Chem. Phys. **123**, 044502 (2005).

[54]A. L. Dobryakov and N. P. Ernsting, "Lineshapes for resonant impulsive stimulated Raman scattering with chirped pump and supercontinuum probe pulses," J. Chem. Phys. **129**, 184504 (2008).

[55]A. A. Granovsky, Firefly v. 8.2, http://classic.chem.msu.su/gran/firefly/index.html.

[56]S. A. Kovalenko, A. L. Dobryakov, J. Ruthmann, and N. P. Ernsting, "Femtosecond spectroscopy of condensed phases with chirped supercontinuum probing," Phys. Rev. A **59**, 2369–2384 (1999).

[57]S. A. Kovalenko, R. Schanz, H. Hennig, and N. P. Ernsting, "Cooling dynamics of an optically excited molecular probe in solution from broadband transient absorption spectroscopy," J. Chem. Phys. **115**, 3256–3273 (2001).

[58]J. Moreno, A. L. Dobryakov, I. N. Ioffe, A. A. Granovsky, S. Hecht, and S. A. Kovalenko, "Broadband transient absorption spectroscopy with 1- and 2-photon excitation," J. Chem. Phys. **143**, 024311 (2015).

[59]O. A. Krohn, M. Quick, S. M. Sudarkova, I. N. Ioffe, C. Richter, and S. A. Kovalenko, "Photoisomerization dynamics of *trans–trans*, *cis–trans* and *cis–cis* diphenylbutadiene from broadband transient absorption spectroscopy and calculations," J. Chem. Phys. **152**, 224305 (2020).

[60]R. D. Jonson III, K. K. Irikura, R. N. Kacker, and R. Kessel, "Scaling factors and uncertainties for ab inito anharmonic vibrational frequencies," J. Chem. Theory Comput. **6**, 2822–2828 (2010).